TU Delft

Delft University of Technology

Classification of hemodynamically significant stenoses from dynamic CT perfusion and CTA myocardial territories

Giordano, Marco; Poot, Dirk; Coenen, Adriaan; van Walsum, Theo; Tezza, Michela; Nieman, Koen; Niessen, Wiro

DOI
10.1002/mp.12126

Publication date
2017

Document Version
Accepted author manuscript

Published in
Medical Physics

Citation (APA)
Giordano, M., Poot, D., Coenen, A., van Walsum, T., Tezza, M., Nieman, K., & Niessen, W. (2017). Classification of hemodynamically significant stenoses from dynamic CT perfusion and CTA myocardial territories. *Medical Physics*, *44*(4), 1347-1358. https://doi.org/10.1002/mp.12126

Important note
To cite this publication, please use the final published version (if applicable).
Please check the document version above.

Copyright
Other than for strictly personal use, it is not permitted to download, forward or distribute the text or part of it, without the consent of the author(s) and/or copyright holder(s), unless the work is under an open content license such as Creative Commons.

Takedown policy
Please contact us and provide details if you believe this document breaches copyrights.
We will remove access to the work immediately and investigate your claim.

This work is downloaded from Delft University of Technology.
For technical reasons the number of authors shown on this cover page is limited to a maximum of 10.

Classification of hemodynamically significant stenoses from dynamic CT perfusion and CTA myocardial territories

[a)] Marco Giordano,[1,2] Dirk H.J. Poot,[1,2] Adriaan Coenen,[3] Theo van Walsum,[2] Michela Tezza,[4] Koen Nieman,[3] and Wiro J. Niessen[1,2]

[1)] *TU Delft, Department of Imaging Physics, Lorentzweg 1, 2628CJ Delft, Netherlands*

[2)] *Biomedical Imaging Group Rotterdam, Department of Radiology & Nuclear Medicine and Department of Medical Informatics, Erasmus MC, University Medical Center Rotterdam, 's Gravendijkwal 230, 3015 CE, Rotterdam, Netherlands*

[3)] *Department of Radiology and Cardiology, Erasmus MC, University Medical Center Rotterdam, 's Gravendijkwal 230, 3015CE Rotterdam, Netherlands*

[4)] *Istituto di Radiologia, Universitá di Verona, Policlinico G.B. Rossi, P.le L.A. Scuro 10, 37134, Verona, Italy*

[a)] Corresponding author: marco.giord@gmail.com

Purpose: Myocardial blood flow (MBF) obtained by dynamic CT perfusion (CTP) has been recently introduced to assess hemodynamic significance of coronary stenosis in coronary artery disease. The diagnostic performance of dynamic CTP MBF is limited due to subjective interpretation of MBF maps and MBF variations caused by physiological, methodological and technical issues. In this paper we introduce a novel method to quantify the hypoperfused volume (HPV) in myocardial territories derived from CT angiography (CTA) in order to overcome the limitations of current dynamic CTP MBF analysis methods.

Methods: The diagnostic performance of HPV in classifying significant stenoses was evaluated on 22 patients (57 vessels) that underwent CTA, CTP and invasive fractional flow reserve (FFR). FFR was used as the standard of reference to determine stenosis significance. The diagnostic performance was compared to that of the mean MBF computed in regions manually annotated by an expert (MA-MBF). HPV was derived by thresholding the MBF in myocardial territories constructed from CTA by locating the closest artery. Diagnostic performance was evaluated using leave-one-case out cross validation. Inter-observer reproducibility was assessed by performing annotations of coronary seeds (HPV) and manual regions (MA-MBF) with two users. Additionally, the influence of different parameter settings on the diagnostic performance of HPV was assessed.

Results: Leave-one-case out cross validation showed that HPV has an accuracy of 72%(58%-83%) with sensitivity of 72%(47%-90%) and specificity of 72%(58%-83%). The accuracy of MA-MBF was 70%(57%-82%) with a sensitivity of 50%(26%-74%) and a specificity of 79%(64%-91%). The Spearman correlation and the kappa statistic was (ρ=0.94, κ=0.86) for HPV and (ρ=0.72, κ=0.82) for MA-MBF. The influence of parameter settings on HPV based diagnostic performance was not significant.

Conclusions: The proposed HPV accurately classifies hemodynamically significant stenoses with a level of accuracy comparable to the mean MBF in regions annotated by an expert. HPV improves inter-observer reproducibility as compared to MA-MBF by providing a more objective criterion to associate the stenotic coronary with the

supplied myocardial territory.

Keywords: Myocardial blood flow; dynamic CT perfusion; coronary CTA; fractional flow reserve; coronary stenosis

I. INTRODUCTION

Coronary computed tomography angiography (CTA) has become an established non-invasive imaging technique to assess coronary artery disease (CAD)[1]. In a CTA scan a single motion-free 3D reconstruction of the heart and coronary arteries is performed to allow evaluation of coronary stenoses (i.e. narrowing). The severity of a stenosis is however a poor predictor of functional significance, especially in lesions of intermediate severity (30%-70% reduction of diameter)[2]. The current standard to assess functional significance of a stenosis is fractional flow reserve (FFR)[3]. FFR is currently regarded as the decisive parameter for revascularization and is assessed during invasive coronary angiography (ICA) by advancing a pressure wire in the stenotic coronary and measuring the pressure difference across the stenosis.

Dynamic stress myocardial CT perfusion (CTP) is a non-invasive imaging technique recently introduced to quantify the myocardial blood flow (MBF)[4]. In a typical myocardial CTP scan, a time-sequence of cardiac images is acquired at ECG-triggered intervals after a short bolus injection. Time-attenuation curves, describing the temporal contrast concentration, are extracted from the reconstructed sequence and successively processed with mathematical models to calculate the MBF. Bamberg *et al.*[5] and Rossi *et al.*[6] demonstrated that the MBF can be used to classify hemodynamically significant stenoses, as defined with FFR, by using cutoff values of 75ml/100ml/min. Kono *et al.*[7] showed that the use of MBF relative to a reference MBF calculated in remote regions improves classification performance compared to using the absolute MBF. Absolute MBF quantification is in fact hampered by MBF variations which might be caused by different physiological conditions[8] and methodological issues such as limited temporal sampling[9] and beam hardening[10]. Kono found an optimal cutoff value of 103 ml/100ml/min for the absolute MBF and 0.85 for the relative MBF.

The above studies are based on mean MBF values calculated in regions manually annotated on the MBF maps. Based on previous experience, the reader draws a region surrounding the suspected myocardial perfusion defect associated with the coronary stenosis of interest. The association between stenosis and affected myocardium is difficult to reproduce and is prone to errors due to the large variations in the coronary anatomy and poor anatomical information in the MBF map. Kirsli *et al.* introduced a framework for combined

visualization of CTA-derived coronaries and 2D perfusion bull's eye map derived from MR[11] and SPECT[12]. Le *et al.*[13] introduced a method to determine the myocardial territory fed by a coronary by proximity to the coronary vessel. The method was evaluated on radio-opaque polymer casts of porcine hearts imaged with micro-CT. Akira *et al.*[14] proposed to determine the myocardial area at risk (MAAR) related to a stenosis in order to predict the MAAR as determined by SPECT perfusion. Their method was based on a voronoi partition of the myocardium from the coronary centerlines. Good correlation of the CTA-derived MAAR with SPECT-derived MAAR was shown, however the capability of CTA-derived MAAR to predict hemodynamic significance was not investigated.

In this paper we introduce hypoperfused volume (HPV) as a novel feature for classification of hemodynamically significant stenoses. The HPV measures the volume of hypoperfused tissue in the myocardial territories distal to the suspected stenosis. HPV is computed semi-automatically from dynamic CTP MBF maps and CTA for each coronary vessel thus enabling direct and objective assessment of the stenosis. As the HPV is evaluated in the myocardial territory associated with a stenosis, artifacts (e.g. beam hardening, motion) present elsewhere in the MBF map, have less influence on the stenosis assessment. Furthermore HPV is derived from the relative MBF thus it is less affected by inter-patient MBF variations. The contributions of this paper are the following: i) HPV as novel feature for classification of hemodynamically significant stenoses ii) a semi-automatic method to calculate the HPV from a set of coronary seeds in CTA and a dynamic CTP MBF map iii) validation of the HPV as feature for classification of significant stenosis using invasive FFR as reference; iv) evaluation of accuracy and reproducibility of HPV as compared to the current standard: the mean MBF calculated in regions manually annotated by an expert v) investigation of the influence of different parameter settings on the diagnostic performance of HPV.

II. METHOD

The aim of this study is to introduce a novel HPV feature for non-invasive classification of hemodynamically significant stenoses from dynamic CTP MBF maps. In this section a semi-automatic method is introduced to calculate HPV from the MBF maps combined with myocardial territories derived from CTA.

Symbols (images in ***bold***)	Meaning
$\boldsymbol{MBF}$	Myocardial blood flow map
$\boldsymbol{CTA}$	CT angiography image
$\boldsymbol{CTA}_{(\mathrm{Aff})}$, $\boldsymbol{CTA}_{(\mathrm{Ela})}$	affine and elastically registered $\boldsymbol{CTA}$
$\boldsymbol{CTP}$	CT perfusion image sequence
$\boldsymbol{CTP}_{(\mathrm{ref})}$	reference image frame of $\boldsymbol{CTP}$
$\boldsymbol{CTP}_{(\mathrm{mask})}$	mask in which $\boldsymbol{MBF}$ is calculated
$\boldsymbol{CTA}^{\boldsymbol{L}}$, $\boldsymbol{CTP}^{\boldsymbol{L}}$	label image with all myocardial territories in $\boldsymbol{CTA}$ and in $\boldsymbol{CTP}$
$\boldsymbol{CTA}^{\boldsymbol{L_k}}$	mask with k-th myocardial territory
$\boldsymbol{CTA}^{\boldsymbol{L_k}}_{(\mathrm{Aff})}$, $\boldsymbol{CTA}^{\boldsymbol{L_k}}_{(\mathrm{Ela})}$	affine and elastically registered k-th myocardial territory
$\boldsymbol{CTP}^{\boldsymbol{L_k}}$	mask with k-th (approximated) myocardial territory in $\boldsymbol{CTP}$
MBF_L, MBF_H	low and high artifact removal thresholds
$\boldsymbol{rMBF}$	relative $\boldsymbol{MBF}$ map
MBF_R	MBF reference value for $\boldsymbol{rMBF}$ calculation
$\boldsymbol{AR}_{(\mathrm{mask})}$	artifacts removal mask
$\boldsymbol{HPV}_{(\mathrm{mask})}$, $\boldsymbol{HPV}_{(\mathrm{open})}$	mask of hypoperfused voxels before and after morphological opening
R_H	relative MBF threshold for $\boldsymbol{HPV}_{(\mathrm{mask})}$ calculation
HPV^{L_k}	hypoperfused volume in k-th myocardial territory
HPV^{vessel}	(feature) hypoperfused volume in main coronary (i.e. LAD)
$\boldsymbol{T}_{(\mathrm{Aff})}$, $\boldsymbol{T}_{(\mathrm{Ela})}$	affine and elastic transformation

TABLE I. Abbreviations and symbols used in the paper

A. Study design

Clinical and imaging data were collected from a prospective study performed at Erasmus MC, University Medical Center, Rotterdam[6]. Patients with suspected CAD underwent CTA and dynamic CTP prior to ICA. FFR was measured during the procedure in the suspected stenotic coronary vessels. Inclusion criteria are fully defined in[6]. Subsequently, from the 48 cases of the prospective study, a subset of 22 cases was selected based on availability of at least two vessels with FFR measurements and presence of at least 1 non-significant stenotic vessel. Cases with 3 vessel disease were excluded due to lack of reference MBF values. Visual inspection was performed to exclude cases with severe motion artifacts that prevent reliable MBF quantification (section II C 4). No such cases were present in the subset.

B. Image acquisition

Single phase CTA scans were performed on a dual-source CT system (Definition Flash-Force; Siemens, Forchheim, Germany) using 90 to 100 mL of iopromide (Ultravist, 370

mgI/mL; Bayer, Berlin, Germany), injected at 5 to 6 mL/s, followed by a saline flush of 45 mL at the same rate. β-blockers were administrated in patients with a fast heart rate. Scan parameters were as follows: ECG-triggered spiral scan mode, tube voltage of 100 kV and 370 mAs per rotation. The reconstruction parameters were: slice thickness 0.4 mm, in plane resolution 0.35 mm; medium-smooth cardiac kernel; the optimal cardiac phase was selected automatically by the workstation's software (Syngo Via, Siemens, Forchheim, Germany) and checked visually by looking for maximum sharpness of coronary contours. The optimal phase resulted mostly in mid-diastole or end-systole.

Dynamic CTP was performed 10 minutes after CTA. After adenosine infusion (140 μg/kg/min for 3 minutes), a bolus of 50 mL was injected at a rate of 6 mL/s, followed by a 40-mL saline flush. An ECG triggered axial scan mode with two alternating table positions[4] was used to repetitively cover the left ventricle myocardium during end systole. Scanning parameters were as follows: tube voltage 100 kV (300 mAS per rotation) in 20 patients and 70 Kv in 2 patients. Images were acquired for a period of 30 seconds while the patient maintained an inspiratory breath hold. $\boldsymbol{CTP}$ images were reconstructed with a 2 mm thickness and in plane resolution of 0.35 mm using a medium-smooth kernel. Prior to MBF calculation, breathing and cardiac motion was corrected using non rigid registration. After registration, the left ventricle myocardium was segmented by performing thresholding on a selected frame (i.e. $\boldsymbol{CTP}_{(\mathrm{ref})}$) resulting in $\boldsymbol{CTP}_{(\mathrm{mask})}$. The $\boldsymbol{MBF}$ was calculated in $\boldsymbol{CTP}_{(\mathrm{mask})}$ as the maximum slope of the fitted myocardial time-attenuation curve divided by the maximum arterial input function. The fitting was achieved by parametric deconvolution[4] assuming a 2-compartment model. Registration, segmentation and $\boldsymbol{MBF}$ calculation were performed using a dedicated software (Volume Perfusion CT Body; Siemens, Forchheim, Germany).

C. Image analysis

In this section we describe the processing steps to calculate the HPV. The idea behind the HPV is to threshold the $\boldsymbol{MBF}$ in the myocardial territories distal to the coronary stenosis. The main assumption is that hemodynamic significance is associated with larger hypoperfused volumes in the myocardial territories distal to the stenosis. The myocardial territories are determined semi-automatically from $\boldsymbol{CTA}$ by locating the closest coronary

within the myocardium. The HPV calculation consists of the following processing steps (figure 1): i) coronary centerlines extraction in ***CTA***, (ii) multi atlas segmentation of the myocardium in ***CTA*** (iii) determination of myocardial territories in ***CTA*** by minimum distance with the coronary centerlines, (iv) registration of the myocardial territories to the ***MBF*** map (v) calculation of the HPV from the registered myocardial territories and the ***MBF***. The HPV is calculated in the main coronary vessels: right coronary artery (RCA), left anterior descending (LAD) and left circumflex (LCX). In the following sections each step is described in more detail.

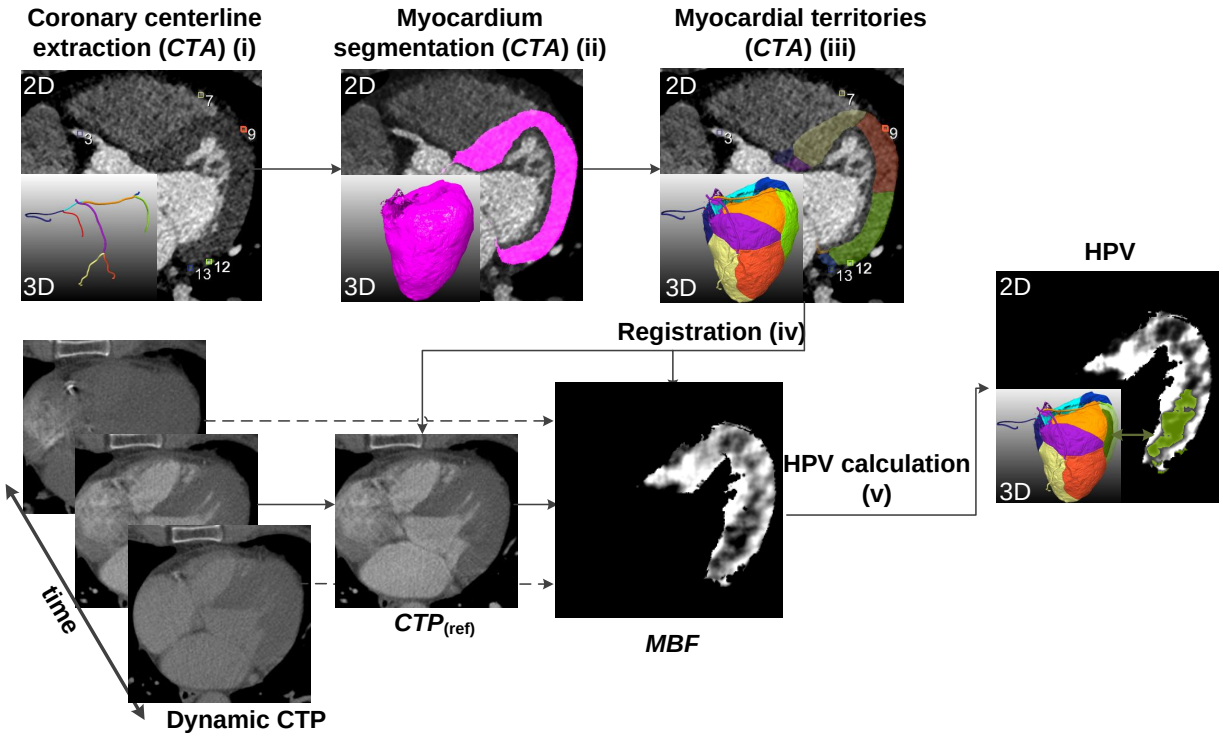


FIG. 1. Image analysis workflow.

1. *Coronary centerlines extraction*

The coronary centerlines are extracted from the ***CTA*** by applying a semi-automatic extraction algorithm based on the minimum cost path. The workflow for the coronary centerlines extraction consists of:

- First, as introduced in[15], a cost image is calculated from ***CTA*** using a multiscale vesselness measure[16] modulated with an intensity threshold function.

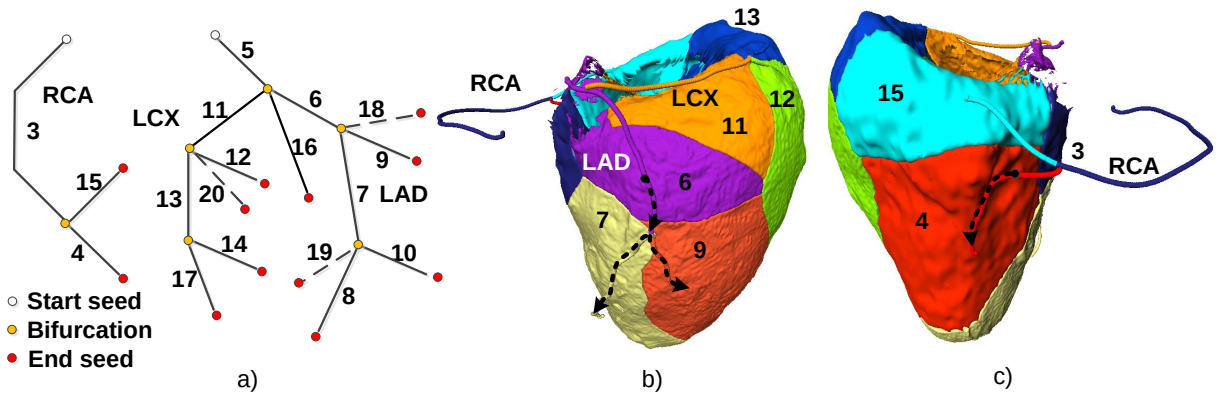


FIG. 2. (a) Model and nomenclature used for start seeds (white), bifurcations (yellow) and end seeds (red). (b)(c) Examples of 3D coronary centerlines and corresponding myocardial territories for LAD (b), LCX (b) and RCA (c). The black dots in b) and c) indicate stenosis points in LAD and RCA respectively. The dashed arrows distal to the stenosis indicate the subsegments affected by the stenosis.

- Then the user defines seeds at the start, bifurcation and end point of the main coronary vessels according to a modification of the myocardial model defined in[17] (figure 2(a)).

- The centerlines are formed by connecting consecutive seeds on the vascular tree through subsegments (see numbered subsegments in figure 2(a)). Each subsegment is extracted by applying a minimum cost path algorithm on the cost image between consecutive seeds[15]. Each extracted subsegment is represented with a set of ordered points $p_{k,m}$ with subsegment index $k \in 1 \dots K$ and point index $m \in 1 \dots M_k$, where K is the number of subsegments and M_k the number of points in subsegment k. In case of erroneous vessel detection, manual definition and/or correction of points is performed.

- Finally, the user selects a 'stenosis point' for each affected main coronary vessel as the most proximal suspected stenosis in the subsegment where FFR was measured. The affected myocardium is determined as the territory distal to the 'stenosis point' below an MBF threshold (section II C 5).

An application enabling the seed annotations and the centerline extractions was implemented in MevisLab (`http://www.mevislab.de/`).

2. Myocardium segmentation

The myocardium is segmented with a validated multi atlas segmentation method[18]. The atlases used in our study were the same used in[18]. The segmentation algorithm and the optimal settings are available at `www.bigr.nl/heartin3d/`.

3. Myocardial territories

The myocardial territories are defined as the myocardial areas fed by specific coronary subsegments. We approximate the myocardial territories as the areas which are the closest, in terms of euclidean distance, to the coronary subsegments. The myocardial territory fed by subsegment k is represented by the binary image $\boldsymbol{CTA^{L_k}}$, which is 1 in the myocardial area where one of the points $p_{k,m}$ is closer than any other point $p_{n,m}$ with $n \neq k$, and 0 everywhere else. In practice each voxel is assigned exclusively to one coronary subsegment. The closest point to a voxel is determined using approximate nearest neighbor search[19].

4. Registration of myocardial territories to MBF maps

To analyze the $\boldsymbol{MBF}$ within the myocardial territories, the myocardial territories have to be spatially aligned to the $\boldsymbol{MBF}$ map for which we use a non-rigid registration approach. The myocardial territories $\boldsymbol{CTA^{L_k}}$ can not be directly registered to the $\boldsymbol{MBF}$ due to insufficient anatomical features in the $\boldsymbol{MBF}$. Hence the $\boldsymbol{CTA}$ image is registered to the $\boldsymbol{CTP}_{(\text{ref})}$ that is aligned with the $\boldsymbol{MBF}$. The resulting transformation is used to deform the $\boldsymbol{CTA^{L_k}}$'s. Cases where no suitable frame $\boldsymbol{CTP}_{(\text{ref})}$ could be aligned with the $\boldsymbol{MBF}$ due to severe motion artifacts were excluded. The registration of the $\boldsymbol{CTA}$ to the to $\boldsymbol{CTP}_{(\text{ref})}$ presents the following challenges:

1. $\boldsymbol{CTA}$ is acquired in mid-diastole or end-systole while $\boldsymbol{CTP}_{(\text{ref})}$ is acquired in end-systole thus there might be substantial non-rigid deformation between these two scans.

2. $\boldsymbol{CTA}$ and $\boldsymbol{CTP}_{(\text{ref})}$ present large contrast differences especially in the interventricular septum: in $\boldsymbol{CTP}_{(\text{ref})}$ (figure 3(b)) the septum is well visible due to the contrast present in both ventricles whereas in $\boldsymbol{CTA}$ (figure 3(a)) the septum's detection is challenging due to the low contrast in the right ventricle. This difference in contrast can cause

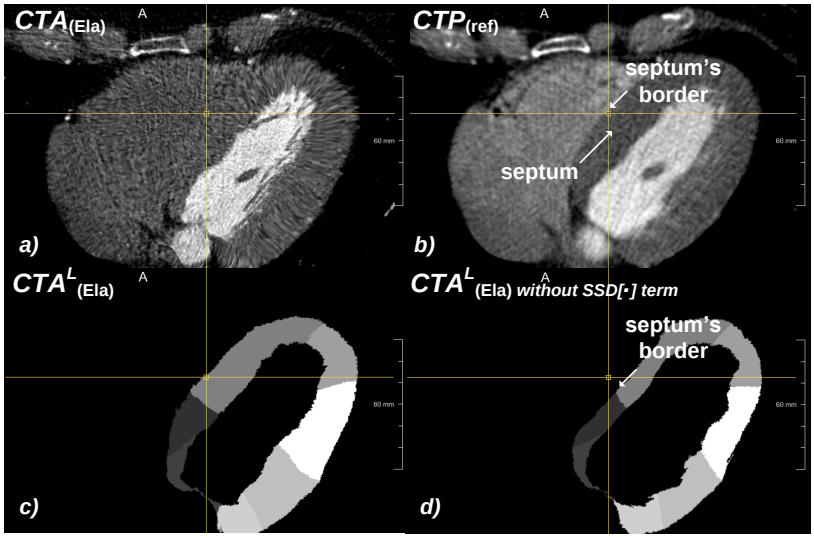


FIG. 3. a) Registered image $\boldsymbol{CTA}_{(\mathrm{Ela})}$ obtained with the $SSD[\cdot]$ terms in equation 4 [W=500HU,L=200HU]. b) Fixed image $\boldsymbol{CTP}_{(\mathrm{ref})}$ [W=500HU,L=200HU]. The yellow square indicates the septum's border c) Registered myocardial territory image $\boldsymbol{CTA}^{\boldsymbol{L}}_{(\mathrm{Ela})}$ obtained with the $SSD[\cdot]$ terms. $\boldsymbol{CTA}^{\boldsymbol{L}}_{(\mathrm{Ela})}$ is obtained by merging all myocardial territories $\boldsymbol{CTA}^{\boldsymbol{L_k}}_{(\mathrm{Ela})}$. d) Registered myocardial territory image $\boldsymbol{CTA}^{\boldsymbol{L}}_{(\mathrm{Ela})}$ obtained without the $SSD[\cdot]$ terms. Here the septum border (white arrow) is misplaced towards the ventricle.

the erroneous registration of the right ventricle into the septum and the subsequent shifting of the septum's border towards the left ventricle. This effect is illustrated in figure 3(d) where the septum's border is moved further towards the left ventricle with respect to the true location indicated by the intersection of the yellow lines.

These challenges are addressed as follows:

1. non-rigid registration is performed to capture the heart deformation. First, an affine registration is performed to align the center of mass and orientation of the images; second, a non-rigid registration is performed to accurately match myocardial borders and myocardial territories. To avoid large deformations and misplacement of myocardial territories a regularization term is used which accounts for the approximate location of the myocardial territories.

2. the use of the myocardial territories $\boldsymbol{CTA}^{\boldsymbol{L_k}}$ in the registration allows localization of

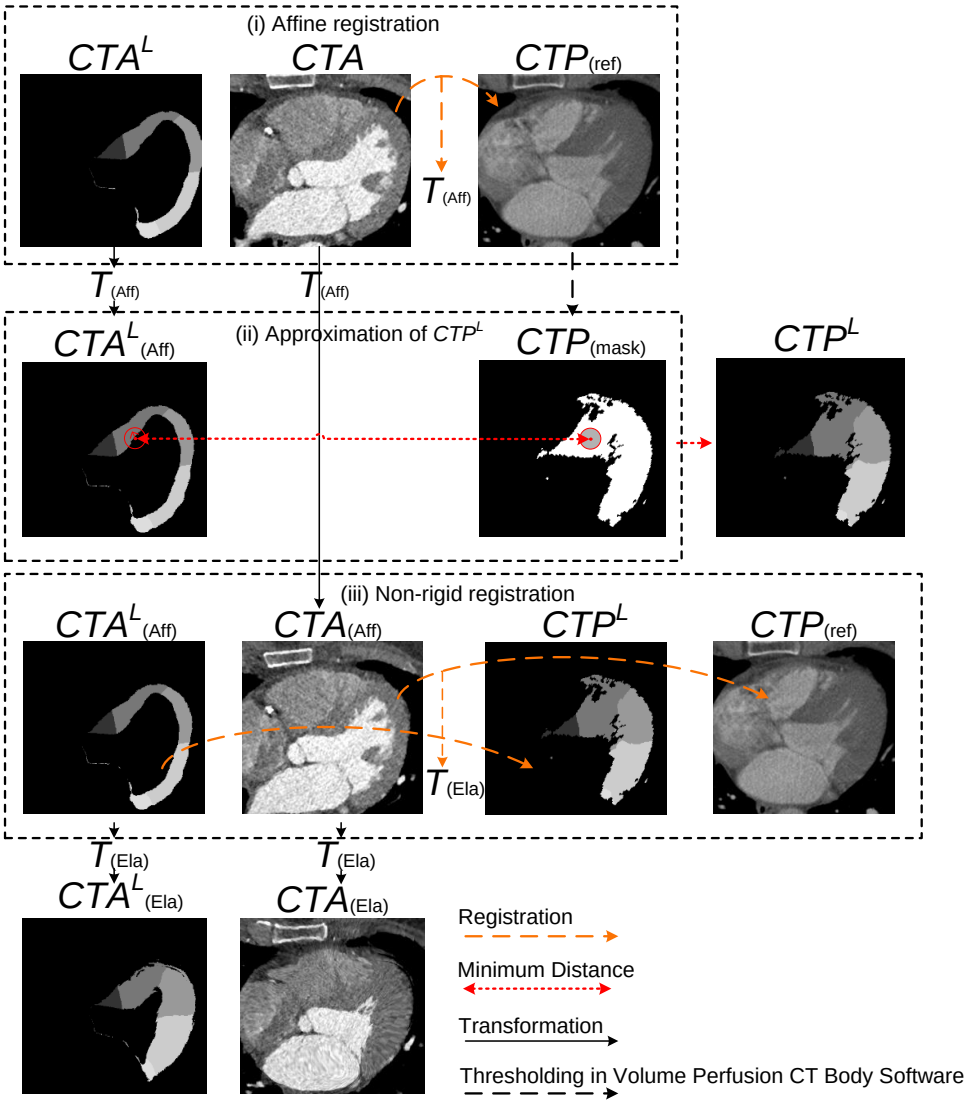


FIG. 4. Workflow for the registration of $\boldsymbol{CTA}$ to $\boldsymbol{CTP}_{(\mathrm{ref})}$. $\boldsymbol{CTA^L}$ is formed by assigning to each $\boldsymbol{CTA^{L_k}}$ its index k and merging them in one image. i) Affine registration of $\boldsymbol{CTA}$ to $\boldsymbol{CTP}_{(\mathrm{ref})}$. ii) Approximation of myocardial territories $\boldsymbol{CTP^{L_k}}$ by minimum distance to the $\boldsymbol{CTA}^{\boldsymbol{L_k}}_{(\mathrm{Aff})}$s. iii) Non-rigid registration of $\boldsymbol{CTA}_{(\mathrm{Aff})}$ and $\boldsymbol{CTA}^{\boldsymbol{L}}_{(\mathrm{Aff})}$ to $\boldsymbol{CTP}_{(\mathrm{ref})}$ and $\boldsymbol{CTP^L}$. $\boldsymbol{CTA}^{\boldsymbol{L}}_{(\mathrm{Aff})}$, $\boldsymbol{CTP^L}$ and $\boldsymbol{CTA}^{\boldsymbol{L}}_{(\mathrm{Ela})}$ are formed similarly as $\boldsymbol{CTA^L}$ by merging the respective myocardial territories.

the interseptum in both $\boldsymbol{CTA}$ and $\boldsymbol{CTP}_{(\mathrm{ref})}$ thus improving the registration of the septum's border.

To describe our registration method we first define a registration in general as a minimization problem:

$$\boldsymbol{T}_{(\mathrm{Gen})} \equiv \arg\min_{\boldsymbol{T}}\{C[I_f(\boldsymbol{x}), I_m(\boldsymbol{T}(\boldsymbol{x}))]\} \tag{1}$$

where $I_f(\boldsymbol{x})$ is the intensity of the fixed image at location $\boldsymbol{x}$, $I_m(\boldsymbol{T}(\boldsymbol{x}))$ is the intensity of the moving image at the transformed location $\boldsymbol{T}(\boldsymbol{x})$, C is the cost function and $\boldsymbol{T}_{(\mathrm{Gen})}$ the final transformation[20]. The method to register $\boldsymbol{CTA}$ to $\boldsymbol{CTP}_{(\mathrm{ref})}$ consists of the following steps (see figure 4):

i) First an affine registration of $\boldsymbol{CTA}$ to $\boldsymbol{CTP}_{(\mathrm{ref})}$ is performed:

$$\boldsymbol{T}_{(\mathrm{Aff})} \equiv \arg\min_{T}\{MI[CTP_{(\mathrm{ref})}(\boldsymbol{x}), CTA(\boldsymbol{T}(\boldsymbol{x}))]\}, \tag{2}$$

where $MI[\cdot]$ is the negated mutual information. The resulting $\boldsymbol{T}_{(\mathrm{Aff})}$ is successively used to obtain the affine transformed myocardial territories $\boldsymbol{CTA}^{\boldsymbol{L_k}}_{(\mathrm{Aff})}$ and the affine transformed image $\boldsymbol{CTA}_{(\mathrm{Aff})}$. Differences in slice thickness were addressed by downsampling the $\boldsymbol{CTA}$ image to the $\boldsymbol{CTP}_{(\mathrm{ref})}$ image grid.

ii) Second, an approximation of the myocardial territories $\boldsymbol{CTP}^{\boldsymbol{L_k}}$ aligned with $\boldsymbol{CTP}_{(\mathrm{ref})}$ is found by assigning each voxel in $\boldsymbol{CTP}_{(\mathrm{mask})}$ to the closest myocardial territory $\boldsymbol{CTA}^{\boldsymbol{L_k}}_{(\mathrm{Aff})}$ as follows:

$$CTP^{L_k}(\boldsymbol{x}) = \begin{cases} 1 & \text{if} \quad \min_{y\in \boldsymbol{CTA}^{\boldsymbol{L_k}}_{(\mathrm{Aff})}} \|\boldsymbol{x}-\boldsymbol{y}\| < \min_{n\neq k, y\in \boldsymbol{CTA}^{\boldsymbol{L_k}}_{(\mathrm{Aff})}} \|\boldsymbol{x}-\boldsymbol{y}\| \\ 0 & \text{otherwise} \end{cases} \tag{3}$$

where $\|\cdot\|$ indicates the euclidean distance. In equation 3 the closest myocardial territory was retrieved using the signed Maurer distance available in ITK[21,22]. The resulting myocardial territories $\boldsymbol{CTP}^{\boldsymbol{L_k}}$s are 1 in the area corresponding to the k-th myocardial territory and zero anywhere else.

iii) Third, a non-rigid registration of $\boldsymbol{CTA}_{(\mathrm{Aff})}$ to $\boldsymbol{CTP}_{(\mathrm{ref})}$ and of the $\boldsymbol{CTA}^{\boldsymbol{L_k}}_{(\mathrm{Aff})}$ to the $\boldsymbol{CTP}^{\boldsymbol{L_k}}$ is performed:

$$\boldsymbol{T}_{(\text{Ela})} \equiv \arg\min_{T}\{MI[CTP_{(\text{ref})}(\boldsymbol{x}), CTA_{(\text{Aff})}(\boldsymbol{T}(\boldsymbol{x}))] + \lambda \cdot \sum_{k} SSD[CTP^{L_k}(\boldsymbol{x}), CTA^{L_k}_{(\text{Aff})}(\boldsymbol{T}(\boldsymbol{x}))]\} \quad (4)$$

where the $SSD[\cdot]$ terms compute the sum of square differences between the moving territories $\boldsymbol{CTA}^{\boldsymbol{L_k}}_{(\text{Aff})}$ and the fixed territories $\boldsymbol{CTP}^{\boldsymbol{L_k}}$ and thus ensure that the myocardial territories are registered to their approximate location in $\boldsymbol{CTP}_{(\text{ref})}$. The benefit of the $SSD[\cdot]$ terms can be appreciated by comparing the registration with the $SSD[\cdot]$ terms in figure 3(c), where the septum border is correctly registered, with the registration without the $SSD[\cdot]$ in figure 3(d), where the septum border is displaced toward the left ventricle. The weight λ was selected in order to have the same contribution to the metric from both the $MI[\cdot]$ and the $SSD[\cdot]$ terms. Experiments on two testing datasets showed that $\lambda = 1$ allowed to have a similar contribution from both terms. The resulting $\boldsymbol{T}_{(\text{Ela})}$ was used to obtain the registered image $\boldsymbol{CTA}_{(\text{Ela})}$ and the registered myocardial territories $\boldsymbol{CTA}^{\boldsymbol{L_k}}_{(\text{Ela})}$.

The registrations and the transformations were performed with the *elastix* package[20] available at `elastix.isi.uu.nl`. The parameter file used for the registration is available at `http://elastix.bigr.nl/wiki/index.php/Parameter_file_database`. The validation of the registration was performed visually and implicitly in the validation of HPV (section III) as severe errors in the registration would deteriorate HPV accuracy.

5. HPV calculation

The HPV^{vessel} is defined as the total hypoperfused volume distal to the stenosis. To calculate this, first the hypoperfused volumes HPV^{L_k} related to the individual myocardial territories are obtained and then the territories distal to the stenosis are summed together. The HPV^{L_k}s are obtained from $\boldsymbol{MBF}$ as follows (figure 5):

- Artifacts removal: a mask $\boldsymbol{AR}_{(\text{mask})}$ is used to reduce breathing and cardiac motion artifacts in $\boldsymbol{MBF}$. Cardiac and breathing motion typically cause large and/or inconsistent variations of the CT signal during the dynamic scan which might result in extreme values in $\boldsymbol{MBF}$. Some of these artifacts are still present after motion correction and after rejection of subjects with severe motion artifacts. $\boldsymbol{AR}_{(\text{mask})}$ selects the voxels not

affected by motion by selecting all voxels in the interval: $MBF_L < \boldsymbol{MBF} < MBF_H$. In our experiments $MBF_L = 20ml/100ml/min$ and $MBF_H = 220ml/100ml/min$. MBF_H is based on the mean $\boldsymbol{MBF}$ in normal tissue and in artifacts at the edge of the myocardium. Most likely due to administration of β-blockers, the $\boldsymbol{MBF}$ values in our datasets were generally lower than in datasets acquired without β-blockers. As such, MBF_H might have to be increased when β-blockers are not administrated.

- Relative MBF: to correct for $\boldsymbol{MBF}$ variations a relative MBF is calculated as $\boldsymbol{rMBF} = \boldsymbol{MBF}/MBF_R$, where MBF_R is a reference value for which different methods are investigated (section III). The different methods to compute MBF_R were: the mean $\boldsymbol{MBF}$ calculated over the voxels in $\boldsymbol{AR}_{(\text{mask})}$ (HPV-rMBF-M), the peak of the histogram where the histogram is calculated with the MBF values in $\boldsymbol{AR}_{(\text{mask})}$ using a bin width of $2ml/100ml/min$ (HPV-rMBF-PH), and the absolute $\boldsymbol{MBF}$ (HPV-MBF).

- Thresholding: an initial segmentation of the hypoperfused volume $\boldsymbol{HPV}_{(\text{mask})}$ is obtained by selecting all voxels with $\boldsymbol{rMBF} < R_H$. R_H is defined as a percentage of MBF_R. Different R_H's are investigated in section III.

- Opening: in order to remove small regions due to noise, an opening operator[23] with different kernel sizes $O_{(\text{ker})}$ is applied to $\boldsymbol{HPV}_{(\text{mask})}$ resulting in $\boldsymbol{HPV}_{(\text{open})}$. Different kernel sizes are investigated in section III.

- HPV^{L_k} computation: HPV^{L_k} is the volume of $\boldsymbol{HPV}_{(\text{open})}$ in $\boldsymbol{CTA}^{\boldsymbol{L_k}}_{(\text{Ela})}$. To calculate HPV^{L_k}, $\boldsymbol{HPV}_{(\text{open})}$ is intersected with $\boldsymbol{CTA}^{\boldsymbol{L_k}}_{(\text{Ela})}$ (figure 5) and then the volume of all resulting non-zero voxels is summed.

Finally HPV^{vessel} is calculated as the sum of the HPV^{L_k}s distal to the 'stenosis point'. The HPV^{L_k}s proximal to the 'stenosis point' and the HPV^{L_k}s located in branches not affected by the examined stenosis are discarded from the calculation to exclude hypoperfusion caused by artifacts and by stenoses different from the one assessed with FFR. In figure 6 two examples for the calculation of HPV^{LAD} are presented: in figure 6(a) the HPV^{L_k}s are all distal to the 'stenosis point' thus $HPV^{LAD} = HPV^{L_6} + HPV^{L_7} + HPV^{L_9}$ whereas in figure 6(b) only HPV^{L_9} is distal to the stenosis hence $HPV^{LAD} = HPV^{L_9}$.

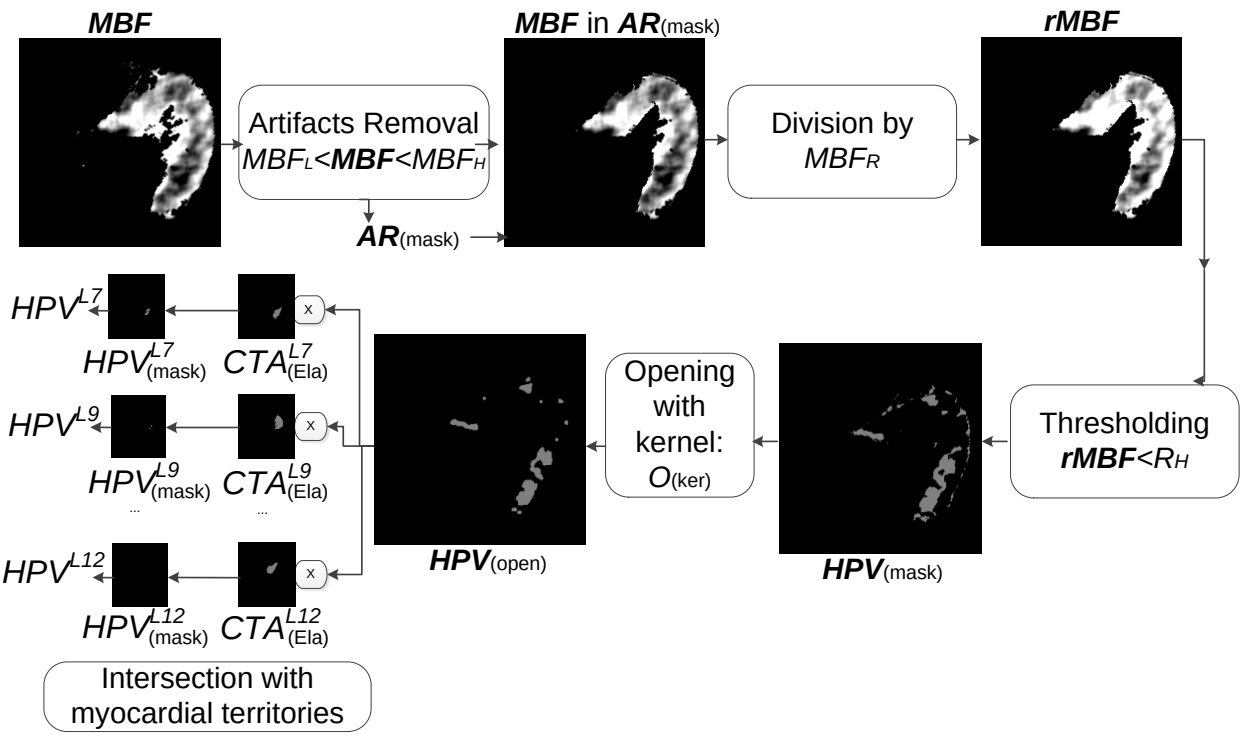


FIG. 5. Calculation of the HPV^{L_k}'s: i) Artifacts removal by applying the mask $\boldsymbol{AR}_{(\mathrm{mask})}$ constructed with the thresholds MBF_{L} and MBF_{H} ii) Division by the reference MBF_R iii) Thresholding by R_H iv) Application of the opening operator with kernel size $O_{(ker)}$ v) Intersection with myocardial territories $\boldsymbol{CTA}^{\boldsymbol{L_k}}_{(\mathrm{Ela})}$ and calculation of HPV^{L_k} volumes.

III. EXPERIMENTS

The aim of our evaluation was to assess the diagnostic performance of HPV for classification of hemodynamically significant stenoses using FFR based classification as reference standard. The diagnostic performance of HPV was compared to that of the mean MBF calculated in regions annotated manually by an expert (MA-MBF). The classification was performed in the RCA, LAD and LCX. In the following, we describe the measurement of invasive FFR and MA-MBF.

A. Invasive FFR

During ICA, angiograms of the left and right coronary arteries were acquired and inspected by the interventional cardiologist to identify suspected coronary lesions. Coronary

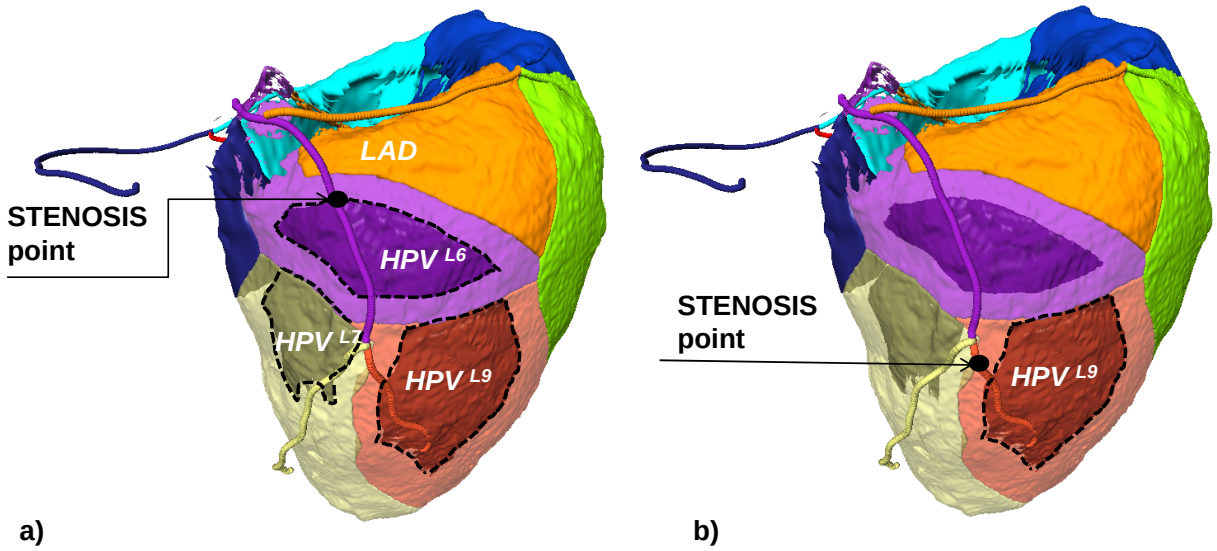


FIG. 6. Examples of evaluation of total hypoperfused volume for LAD: HPV^{LAD}. The dark areas indicate the individual hypoperfused volumes: HPV^{L_6}, HPV^{L_7} and HPV^{L_9} a) In this example all volumes are distal to the stenosis thus the total hypoperfused volume is $HPV^{LAD} = HPV^{L_6} + HPV^{L_7} + HPV^{L_9}$; b) Here only HPV^{L_9} is distal to the stenosis while HPV^{L_6} and HPV^{L_7} are in non-affected branches thus $HPV^{LAD} = HPV^{L_9}$.

lesions with diameter narrowing between 30 and 90% were selected to perform FFR. The FFR was measured using a pressure wire (PressureWire, Radi Medical Systems, Uppsala, Sweden) according to the standard clinical protocol[24] and defined as FFR=(arterial pressure at the site distal to the stenosis)/(arterial pressure at the proximal site or aorta). The FFR measurements were performed at maximal hyperemia induced by a continuous intravenous infusion of adenosine (140 μg/kg/min for a minimum of 2 min). The hemodynamic significance of a stenosis was assumed when FFR$\leq$ 0.8.

B. MA-MBF

The MA-MBF was calculated in regions annotated manually by users with previous experience in dynamic CT MBF analysis. The regions were selected on 2-mm thick short-axis views of the MBF maps. Circular regions of at least 0.5 cm^2 were positioned in each myocardial segment according to a standard 17-segment model[17]. Myocardial segments supplied by the same coronary vessel were considered as part of the same main myocardial

territory (i.e. LAD, LCX and RCA). Within each territory, the myocardial segment with the lowest $\boldsymbol{MBF}$ mean was selected and used in the analysis. Prior to region selection the users inspected the $\boldsymbol{CTA}$.

C. Statistical analysis

The diagnostic performances of HPV and MA-MBF were evaluated by measuring sensitivity, specificity, and the area under the curve (AUC) of the receiving operating curve (ROC)[25]. Continuous variables are presented as mean ± standard deviation or median and 95% confidence interval.

First we investigated the influence of different parameter settings on the diagnostic performance of the HPV. The investigated parameters were: the reference MBF_R (section II C 5), the threshold R_H and the kernel size of the opening operator $O_{(\mathrm{ker})}$ (section II C 5). The investigated R_Hs were 80%, 90%, 100% of MBF_R. For the absolute MBF, the R_Hs were 80, 90, 100 ml/100ml/min. The kernel sizes of the opening operator were $(2 \times 2 \times 2)mm^3$, $(1 \times 1 \times 2)\mathrm{mm}^3$ and the null kernel $(0 \times 0 \times 0)\mathrm{mm}^3$. AUCs were calculated for all the combinations of the 3 settings and the setting yielding the highest AUC (HPV*-setting) was compared to the MA-MBF in terms of sensitivity and specificity. Optimal cut-off values for HPV* and MA-MBF were calculated according to the Youden index[26]. The statistical analysis was performed using MATLAB[27].

Second, leave-one-case out cross-validation was performed to evaluate the capability to assess new cases using settings optimized on previously analyzed cases. In leave-one-out cross validation[28] training is performed on all cases except the test case and then the 'trained' model is used to classify the test case. In our validation, each training stage consists in the following: i) first the HPV is estimated for all combinations of parameter settings similarly as above (MBF_R, R_H and $O_{(\mathrm{ker})}$) ii) for every parameter setting, the ROC is calculated for the estimated HPV and then the cutoff is determined based on the Youden index. iii) among all parameter settings, the setting yielding the highest AUC is selected and used to classify the test case.

Third, the inter-observer reproducibility of HPV and MA-MBF was assessed by the Spearman correlation coefficient, the kappa statistic and the Bland-Altman plot[29] computed on values obtained by two different users. The setting used for both users was HPV*-setting.

Settings analysis (full dataset)	Sensitivity	Specificity	Accuracy	AUC
HPV*	83%(59%-96%)	77%(61%-89%)	79%(66%-89%)	0.84
MA-MBF	72%(47%-90%)	77%(61%-89%)	75%(62%-86%)	0.75
Leave-one-case out cross validation				
HPV	72%(47%-90%)	72%(58%-83%)	72%(58%-83%)	-
MA-MBF	50%(26%-74%)	79%(64%-91%)	70%(57%-82%)	-

TABLE II. Diagnostic performance of HPV and MA-MBF for the settings analysis obtained on the full dataset and for the leave-one-case out cross validation. HPV* is the performance obtained with the HPV*-setting.

The kappa statistic was computed assuming the cutoff of the user who obtained the highest AUC. The users performing the seed annotations had previous experience in cardiac imaging.

IV. RESULTS

The study population included 22 cases with FFR measured in 57 vessels. Among these, 18 were classified as hemodynamically significant (FFR$\leq$ 0.8) and 39 non-significant (FFR$>$ 0.8).

Figure 7 shows results obtained for different parameter settings on the full dataset (22 cases). Figure 7(a)-(c) show AUC values obtained with different MBF_R, different R_Hs, and different kernels $O_{(\mathrm{ker})}$. The horizontal dashed line indicates the highest AUC obtained with the HPV*-setting. The mean AUC was 0.80 (0.79-0.82) for HPV and 0.75 for MA-MBF. The optimal diagnostic performance (AUC=0.84) was obtained with HPV*-setting: HPV-rMBF-M, $R_H = 90\%$, $O_{(\mathrm{ker})} = (0 \times 0 \times 0)$ mm^3. At an optimal cutoff of 12.5 ml the HPV* estimation achieved a sensitivity and specificity of 83% and 77% (confidence intervals reported in table II). At an optimal cut-off of 76.0 ml/100ml/min the MA-MBF achieved a sensitivity and specificity of 72% and 77%. Figure 7(d) shows the ROC obtained for HPV* (dashed line) and for MA-MBF (solid line). Figure 8(a) and 8(b) show HPV* versus FFR and MA-MBF versus FFR, respectively.

Leave-one-case out cross validation results are reported in table II. The most recurrent

HPV parameter setting (59% of the cases) found by the leave-one-case out cross validation was HPV-rMBF-M, $R_H = 90\%$, $O_{(\mathrm{ker})} = (0 \times 0 \times 0)$ mm^3 which was consistent with the HPV*-setting.

The Spearman correlation coefficient and the kappa statistic were ($\rho = 0.94$, $\kappa = 0.86$) for HPV* and ($\rho = 0.72$, $\kappa = 0.82$) for MA-MBF. Figure 9(a) and 9(b) show HPV* of user 1 versus HPV* of user 2 and MA-MBF of user 1 versus the MA-MBF of user 2, respectively. The color used to depict each vessel measurement represents the corresponding FFR: black for significant stenoses and gray for non-significant. The dashed lines indicate the cutoff of HPV* (figure 9(a)) and MA-MBF (figure 9(b)) for user 1. A better separation between significant and non significant stenoses can be observed for HPV* as compared to MA-MBF when comparing the separation in figure 9(a) with the one in figure 9(b). Figure 10(a) and 10(b) show the Bland-Altman plot for HPV* and MA-MBF. The mean difference for HPV* was 0.0±5.0 ml while for MA-MBF it was -1.3±41.9 ml/100ml/min. The mean difference relative to the full range was 0.0%±35.4% for HPV* and -1.2%±75.4% for MA-MBF. The plots showed no significant bias of the differences between users for both methods. For MA-MBF larger differences between users were observed towards higher MBF values. For the HPV* no systematic trends between users were observed.

V. DISCUSSION

HPV was introduced as a novel feature to classify hemodynamically significant stenoses based on dynamic CTP-MBF maps and CTA myocardial territories. In this study HPV was validated against invasive FFR and additionally its diagnostic performance was compared to that of the mean MBF calculated in regions annotated manually by an expert (MA-MBF).

The main results of our study are: i) HPV is capable of classifying hemodynamically significant stenoses with accuracy comparable to that of the mean MBF computed in regions annotated by an expert; ii) HPV is more reproducible than MA-MBF.

The confidence intervals of the performance measures were rather large, owing to the limited size of the current study. A larger study will be required to investigate the difference in performance of HPV and MA-MBF in more detail. Also, it should be noted that the performance of MA-MBF in our leave-one-case out cross validation was lower than that obtained in the prospective study[7]. This can be explained by several factors: the selection

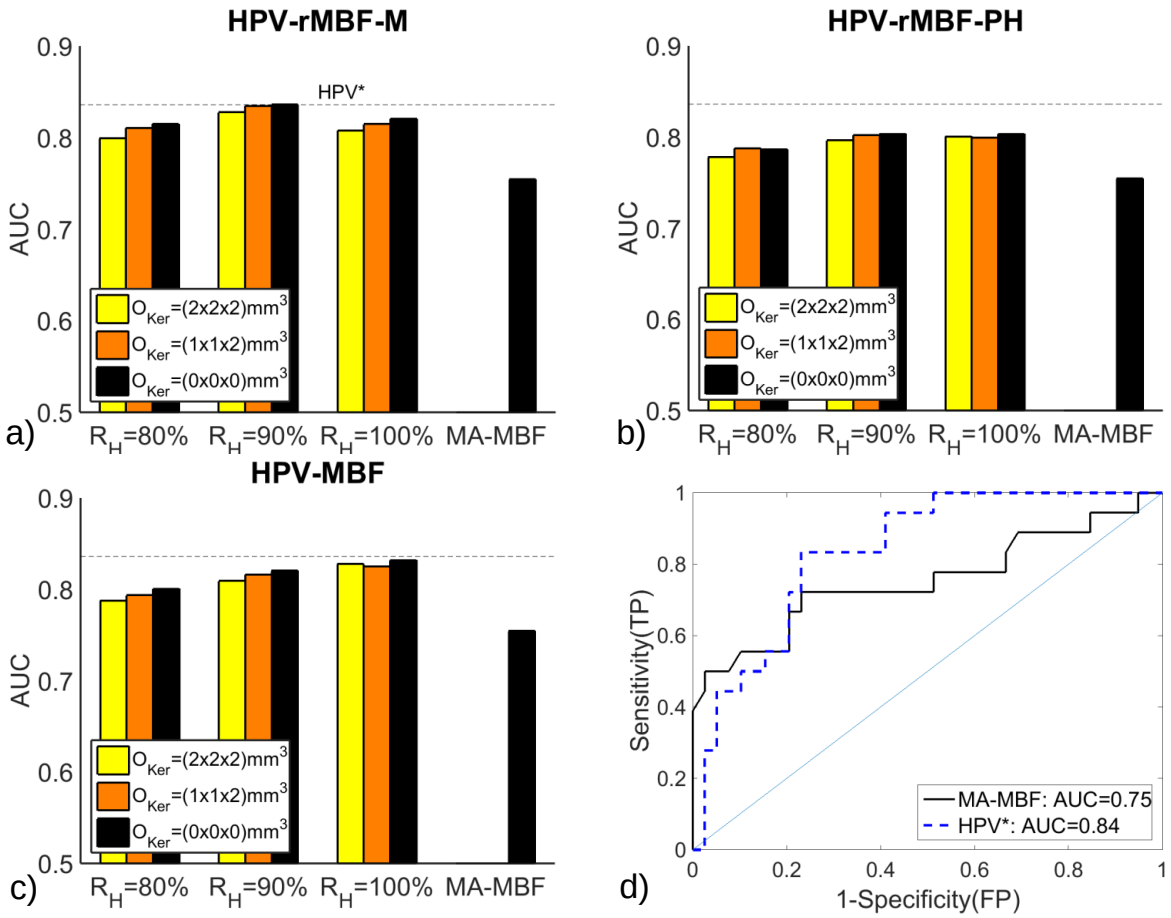
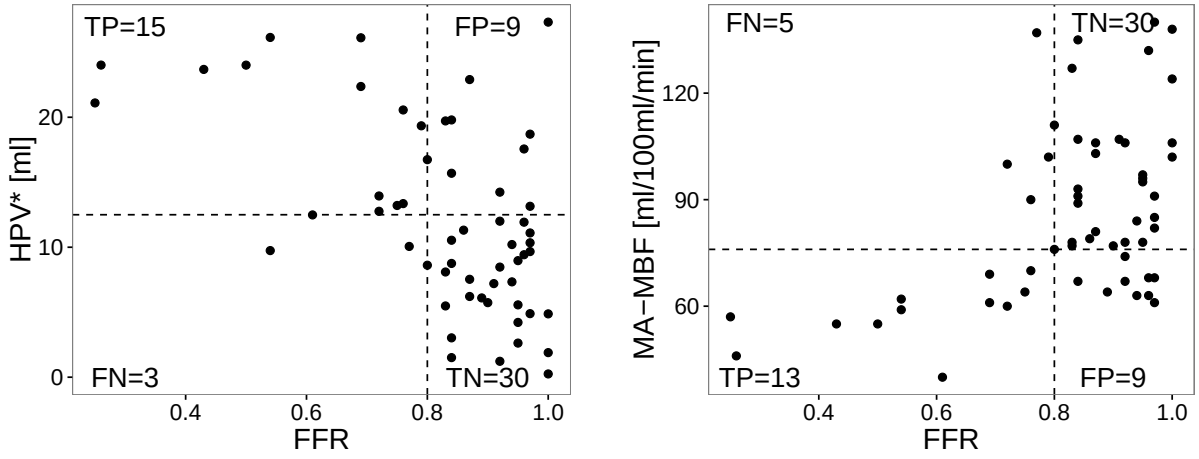


FIG. 7. (a)-(c) Bar plots of the AUC obtained using different parameter settings. Different plots show results obtained with different MBF_Rs: (a) mean MBF (HPV-rMBF-M), (b) peak histogram (HPV-rMBF-PH), (c) absolute MBF (HPV-MBF). Bars are grouped according to the R_T used. The color indicate the kernel size used for the opening operator. The AUC obtained with the MA-MBF is depicted on the right of each bar plot. The horizontal dashed line indicate the highest AUC obtained with HPV*-setting. (d) ROC obtained for HPV* (dashed line) and for MA-MBF (solid line)

of cases, the different observer, the different methods to select the cutoff (Youden versus manual) and the different methods to perform the validation: typically evaluation on the full dataset on which the cutoff was selected, as in[7], gives a more optimistic performance estimate than the leave-one-out cross validation that we used. In cross validation, in fact, the cutoff is optimized for each case separately on a smaller dataset.

With respect to diagnostic performance, even though the performances of HPV and MA-



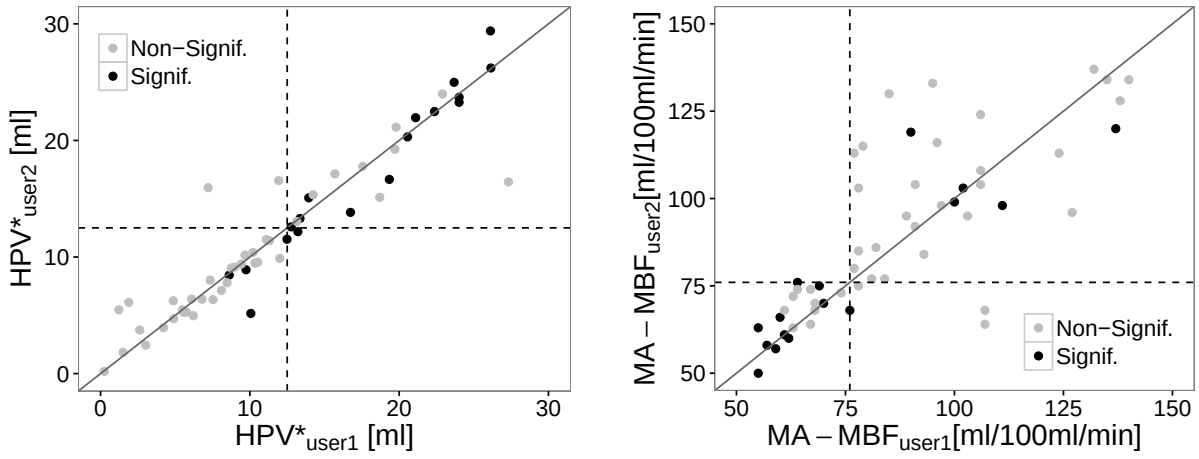
(a) (b)

FIG. 8. (a) HPV* versus FFR: the horizontal line indicates the optimal cutoff for HPV* (12.5 ml). The vertical line indicates the cutoff for FFR (0.8). (b) MA-MBF versus FFR: the horizontal line indicates the cutoff (76.0 ml/100ml/min).

MBF were comparable, HPV has the advantage that it can be obtained by non-experts in dynamic CTP-MBF analysis. In fact, HPV is calculated semi-automatically and does not require the extensive expertise needed to interpret the MBF maps which is a limiting factor for widespread use of dynamic CTP-MBF. The presented results could be obtained by only requiring knowledge of the coronary anatomy in CTA.

Another advantage of HPV as compared to MA-MBF is the higher inter-observer reproducibility which can be attributed to the more objective and systematic criteria to associate the culprit coronary with the affected myocardial territory. In the MA-MBF analysis, this association is performed subjectively by the user who can be influenced by artifacts and/or local MBF variations. Additionally, anatomical variations of the coronary tree between cases can make this association even more challenging because of the different correspondence between myocardial territories and feeding coronary vessels. The time required to place seeds for coronary centerline extraction in HPV was comparable to the time required for the manual annotations in MA-MBF (10-15 min per case) thus HPV does not require additional interaction time.

As concerning the influence of the parameters settings, the analysis showed that most settings do not significantly influence the diagnostic performance of HPV. Only a slight trend

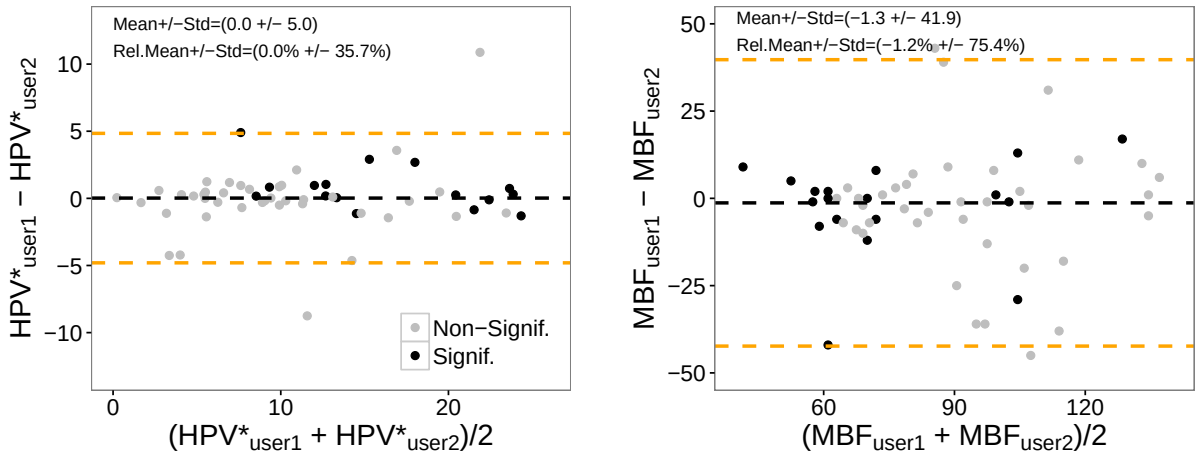


(a) (b)

FIG. 9. (a) HPV* of user 1 versus HPV* of user 2. Each measurement is represented with a different color according to the FFR: black for significant stenoses (FFR≤0.8) and gray for non-significant (FFR>0.8). The dashed lines indicate the cutoff for user 1. Vessels with significant stenosis are ideally located towards the upper right quadrant (i.e high HPV* values). (b) MA-MBF of user 1 versus MA-MBF of user 2. The dashed lines indicate the cutoff for user 1. Significant stenoses are ideally located towards the lower left quadrant (i.e low MA-MBF).

towards better performances for small/null kernel sizes was observed suggesting that the opening operator does not improve the performance. For the considered range of settings, the performance of classification based on HPV was comparable to classification based on MA-MBF and additionally, for the optimal estimation HPV*, there was a promising, but not significant, trend towards higher AUC with respect to MA-MBF (0.84 vs 0.75) (p-value=0.25). This trend was confirmed visually in the inter-observer reproducibility analysis where a more distinct separation between significant and non significant stenoses was achieved by HPV. However, due to the limited sample size the difference in performance between the two methods was not significant. In future, a larger population should be analyzed to evaluate whether HPV can significantly improve classification of significant stenoses with respect to current state of the art MA-MBF.

A limitation of the method is the possible assignment of myocardial territories through anatomical structures that were not modeled like the right ventricle. Currently this can



(a) (b)

FIG. 10. Bland-Altman plot for HPV* (a) and MA-MBF (b) for values obtained with two users. The mean difference ± two standard deviations are indicated by the black and orange lines, respectively. The range on the y axis was adjusted to have a ratio y-axis/x-axis of 1 for both plots. Absolute and relative mean differences ± two standard deviations are reported at the top.

result in inaccurate assignment of RCA subsegments (for instance subsegment 3 in figure 2(b) and (c)) to left ventricle myocardial territories. A possible remedy could be evaluating the distance exclusively within the myocardium mask and adding the right ventricle to the segmentation. Truncation of small coronary vessels (i.e with diameter less then 1.5 mm) is another possible source of error[13]. This is caused by the limited signal to noise ratio of current clinical CT scanners thus it will require a technological improvement to be addressed.

VI. CONCLUSION

We introduced semi-automatically derived hypoperfused volume as a novel feature for non-invasive classification of significant stenoses from dynamic CTP MBF maps and CTA myocardial territories. The feature is extracted with image processing techniques without subjective interpretation and extensive user interaction. The evaluation showed that the proposed feature can accurately classify significant stenoses, as determined by invasive FFR, with comparable accuracy and higher reproducibility than current methods based on manual annotations on MBF maps. These performances were obtained with settings optimized on

a dataset of 22 cases from a single center. In future studies, the performances should be evaluated on a larger dataset also including data from different centers. This would allow to verify the robustness of the settings against MBF variations that might occur due to different scanners and different acquisition conditions.

ACKNOWLEDGEMENTS

This research was funded through the 'Heart in 4D' project, Medical Delta Imaging Institute, ZonMW. Adriaan Coenen and Koen Nieman were supported by the Dutch heart foundation under grant number 2014T061.

DISCLOSURE OF CONFLICT OF INTEREST

Koen Nieman received institutional research support from Siemens Medical Solutions, GE Healthcare, Bayer Healthcare and Heartflow. Wiro Niessen is co-founder, chief scientific officer and shareholder of Quantib BV.

REFERENCES

[1]D. Lloyd-Jones, R. J. Adams, T. M. Brown, M. Carnethon, S. Dai, G. De Simone, T. B. Ferguson, E. Ford, K. Furie, C. Gillespie, *et al.*, "Heart disease and stroke statistics2010 update a report from the american heart association," *Circulation*, vol. 121, no. 7, pp. e46–e215, 2010.

[2]B. W. Meijboom, C. A. Van Mieghem, N. van Pelt, A. Weustink, F. Pugliese, N. R. Mollet, E. Boersma, E. Regar, R. J. van Geuns, P. J. de Jaegere, *et al.*, "Comprehensive assessment of coronary artery stenoses: computed tomography coronary angiography versus conventional coronary angiography and correlation with fractional flow reserve in patients with stable angina," *Journal of the American College of Cardiology*, vol. 52, no. 8, pp. 636–643, 2008.

[3]N. H. Pijls, B. de Bruyne, K. Peels, P. H. van der Voort, H. J. Bonnier, J. Bartunek, and J. J. Koolen, "Measurement of fractional flow reserve to assess the functional severity of coronary-artery stenoses," *New England Journal of Medicine*, vol. 334, no. 26, pp. 1703–1708, 1996.

[4]A. H. Mahnken, E. Klotz, H. Pietsch, B. Schmidt, T. Allmendinger, U. Haberland, W. A. Kalender, and T. Flohr, "Quantitative whole heart stress perfusion ct imaging as noninvasive assessment of hemodynamics in coronary artery stenosis: preliminary animal experience," *Investigative radiology*, vol. 45, no. 6, pp. 298–305, 2010.

[5]F. Bamberg, A. Becker, F. Schwarz, R. P. Marcus, M. Greif, F. von Ziegler, R. Blankstein, U. Hoffmann, W. H. Sommer, V. S. Hoffmann, *et al.*, "Detection of hemodynamically significant coronary artery stenosis: incremental diagnostic value of dynamic ct-based myocardial perfusion imaging," *Radiology*, vol. 260, no. 3, pp. 689–698, 2011.

[6]A. Rossi, A. Dharampal, A. Wragg, L. C. Davies, R. J. van Geuns, C. Anagnostopoulos, E. Klotz, P. Kitslaar, A. Broersen, A. Mathur, *et al.*, "Diagnostic performance of hyperaemic myocardial blood flow index obtained by dynamic computed tomography: does it predict functionally significant coronary lesions?," *European Heart Journal-Cardiovascular Imaging*, vol. 15, no. 1, pp. 85–94, 2014.

[7]A. K. Kono, A. Coenen, M. Lubbers, A. Kurata, A. Rossi, A. Dharampal, M. Dijkshoorn, R.-J. van Geuns, G. P. Krestin, and K. Nieman, "Relative myocardial blood flow by dynamic computed tomographic perfusion imaging predicts hemodynamic significance of coronary stenosis better than absolute blood flow," *Investigative radiology*, vol. 49, no. 12, pp. 801–807, 2014.

[8]A. Rossi, D. Merkus, E. Klotz, N. Mollet, P. J. de Feyter, and G. P. Krestin, "Stress myocardial perfusion: imaging with multidetector ct," *Radiology*, vol. 270, no. 1, pp. 25–46, 2014.

[9]M. Ishida, K. Kitagawa, T. Ichihara, T. Natsume, R. Nakayama, N. Nagasawa, M. Kubooka, T. Ito, M. Uno, Y. Goto, *et al.*, "Underestimation of myocardial blood flow by dynamic perfusion ct: Explanations by two-compartment model analysis and limited temporal sampling of dynamic ct," *Journal of Cardiovascular Computed Tomography*, 2016.

[10]K. Kitagawa, R. T. George, A. Arbab-Zadeh, J. A. Lima, and A. C. Lardo, "Characterization and correction of beam-hardening artifacts during dynamic volume ct assessment of myocardial perfusion 1," *Radiology*, vol. 256, no. 1, pp. 111–118, 2010.

[11]H. A. Kirişli, V. Gupta, S. W. Kirschbaum, A. Rossi, C. Metz, M. Schaap, R. J. van Geuns, N. Mollet, B. P. Lelieveldt, J. H. Reiber, *et al.*, "Comprehensive visualization of multimodal cardiac imaging data for assessment of coronary artery disease: first clinical results of the smartvis tool," *International journal of computer assisted radiology and*

surgery, vol. 7, no. 4, pp. 557–571, 2012.

[12]H. A. Kirişli, V. Gupta, R. Shahzad, I. Al Younis, A. Dharampal, R.-J. van Geuns, A. J. Scholte, M. A. de Graaf, R. M. Joemai, K. Nieman, *et al.*, "Additional diagnostic value of integrated analysis of cardiac cta and spect mpi using the smartvis system in patients with suspected coronary artery disease," *Journal of Nuclear Medicine*, vol. 55, no. 1, pp. 50–57, 2014.

[13]H. Le, J. T. Wong, and S. Molloi, "Estimation of regional myocardial mass at risk based on distal arterial lumen volume and length using 3d micro-ct images," *Computerized Medical Imaging and Graphics*, vol. 32, no. 6, pp. 488–501, 2008.

[14]A. Kurata, A. Kono, T. Sakamoto, T. Kido, T. Mochizuki, H. Higashino, M. Abe, A. Coenen, R. G. Saru-Chelu, P. J. de Feyter, *et al.*, "Quantification of the myocardial area at risk using coronary ct angiography and voronoi algorithm-based myocardial segmentation," *European radiology*, vol. 25, no. 1, pp. 49–57, 2015.

[15]C. Metz, M. Schaap, A. Weustink, N. Mollet, T. van Walsum, and W. Niessen, "Coronary centerline extraction from ct coronary angiography images using a minimum cost path approach," *Medical physics*, vol. 36, no. 12, pp. 5568–5579, 2009.

[16]A. F. Frangi, W. J. Niessen, K. L. Vincken, and M. A. Viergever, "Multiscale vessel enhancement filtering," in *Medical Image Computing and Computer-Assisted Interventation*MICCAI98*, pp. 130–137, Springer, 1998.

[17]M. D. Cerqueira, N. J. Weissman, V. Dilsizian, A. K. Jacobs, S. Kaul, W. K. Laskey, D. J. Pennell, J. A. Rumberger, T. Ryan, M. S. Verani, *et al.*, "Standardized myocardial segmentation and nomenclature for tomographic imaging of the heart a statement for healthcare professionals from the cardiac imaging committee of the council on clinical cardiology of the american heart association," *Circulation*, vol. 105, no. 4, pp. 539–542, 2002.

[18]H. A. Kirişli, M. Schaap, S. Klein, S. Papadopoulou, M. Bonardi, C.-H. Chen, A. Weustink, N. Mollet, E. Vonken, R. van der Geest, *et al.*, "Evaluation of a multi-atlas based method for segmentation of cardiac cta data: a large-scale, multicenter, and multivendor study," *Medical physics*, vol. 37, no. 12, pp. 6279–6291, 2010.

[19]S. Arya, D. M. Mount, N. S. Netanyahu, R. Silverman, and A. Y. Wu, "An optimal algorithm for approximate nearest neighbor searching fixed dimensions," *Journal of the ACM (JACM)*, vol. 45, no. 6, pp. 891–923, 1998.

[20]S. Klein, M. Staring, and J. P. Pluim, "Evaluation of optimization methods for nonrigid medical image registration using mutual information and b-splines," *Image Processing, IEEE Transactions on*, vol. 16, no. 12, pp. 2879–2890, 2007.

[21]C. R. Maurer Jr, R. Qi, and V. Raghavan, "A linear time algorithm for computing exact euclidean distance transforms of binary images in arbitrary dimensions," *Pattern Analysis and Machine Intelligence, IEEE Transactions on*, vol. 25, no. 2, pp. 265–270, 2003.

[22]L. Ibanez, W. Schroeder, L. Ng, J. Cates, the InsightSoftware Consortium, and R. Hamming, "The itk software guide," *Kitware, Inc. (ISBN 1-930934-10-6)*, 2003.

[23]R. M. Haralick and L. G. Shapiro, *Computer and Robot Vision, Volume I*. Addison-Wesley, 1992.

[24]N. Pijls, J. Van Son, R. Kirkeeide, B. De Bruyne, and K. Gould, "Experimental basis of determining maximum coronary, myocardial, and collateral blood flow by pressure measurements for assessing functional stenosis severity before and after percutaneous transluminal coronary angioplasty.," *Circulation*, vol. 87, no. 4, pp. 1354–1367, 1993.

[25]E. R. DeLong, D. M. DeLong, and D. L. Clarke-Pearson, "Comparing the areas under two or more correlated receiver operating characteristic curves: a nonparametric approach," *Biometrics*, pp. 837–845, 1988.

[26]W. J. Youden, "Index for rating diagnostic tests," *Cancer*, vol. 3, no. 1, pp. 32–35, 1950.

[27]MATLAB and S. T. Release, *version 8.4.0 (R2014b)*. Natick, Massachusetts: The MathWorks Inc., 2014.

[28]P. A. Lachenbruch and M. R. Mickey, "Estimation of error rates in discriminant analysis," *Technometrics*, vol. 10, no. 1, pp. 1–11, 1968.

[29]J. M. Bland and D. Altman, "Statistical methods for assessing agreement between two methods of clinical measurement," *The lancet*, vol. 327, no. 8476, pp. 307–310, 1986.